Fuel 424 (2026) 139311

Contents lists available at ScienceDirect

Fuel

journal homepage: www.elsevier.com/locate/fuel

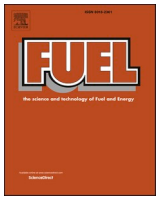

Full Length Article

Study of Ni-YSZ anode under pure and diluted NH_3 conditions towards NO production

Celina Fernandes [a], Laura I.V. Holz [b,c], Francisco J.A. Loureiro [b,c], Sergey M. Mikhalev [b,c], Fátima Santos [a], Duncan P. Fagg [b,c,*], Adélio Mendes [a,**]

[a] LEPABE – Laboratory for Process Engineering, Environment, Biotechnology and Energy, ALiCE – Associate Laboratory in Chemical Engineering, Faculty of Engineering, University of Porto, Rua Dr. Roberto Frias, 4200-465 Porto, Portugal
[b] TEMA – Centre for Mechanical Technology and Automation, Department of Mechanical Engineering, University of Aveiro 3810-193 Aveiro, Portugal
[c] LASI – Intelligent Systems Associate Laboratory, 4800-058 Guimarães, Portugal

ARTICLE INFO

Keywords:
Direct ammonia solid oxide fuel cells
$Sr_2Fe_{1.5}Mo_{0.5}O_{6-\delta}$
Nitrous oxide reduction
Ammonia oxidation
Nitric oxide production

ABSTRACT

Direct ammonia solid oxide fuel cells (DA-SOFCs) have been widely recognized as highly efficient energy conversion devices. Their application to the reduction and valorisation of nitrous oxide (N_2O), a potent greenhouse gas, represents a promising strategy for mitigating global warming while simultaneously addressing energy demands. The present work extends this concept by investigating an $Sr_2Fe_{1.5}Mo_{0.5}O_{6-\delta}$||CGO||YSZ||Ni-YSZ solid oxide fuel cell (SOFC), providing insight into the simultaneous electrochemical reduction of N_2O at the cathode and the electrochemical oxidation of NH_3 at the anode. This approach aligns with the objective of achieving N_2O abatement and valorisation through the production of NO at the anode, a valuable intermediate in the nitric acid synthesis process. In this study, the anodic reaction is examined for different fuel compositions, ranging from pure NH_3 to 6 % of NH_3 balanced in N_2, at an intermediate operating temperature of 750 °C. The results indicate that fuel dilution had no significant impact on the overall electrical performance of the cell, as decreasing the ammonia concentration from pure NH_3 to 10 % NH_3 led to only a moderate reduction in power density, from 75 to 62 mW cm^{-2}. Notably, operation under diluted fuel conditions enabled the electrochemical oxidation of NH_3 to produce NO, which makes operation under diluted conditions attractive. Concurrently, nitrous oxide decomposition at the cathode was *ca.* 10 %, which, although modest, is a promising result considering the high thermal stability of the N_2O molecule.

1. Introduction

Ammonia (NH_3) has been widely considered a promising fuel in the context of decarbonization, particularly when produced from renewable energy sources and used for power generation. Ammonia is of particular interest as as a carbon-free hydrogen carrier becuase, as under appropriate operating conditions and with suitable catalysts, it can be decomposed into hydrogen (H_2) and nitrogen (N_2), making it a viable alternative to direct hydrogen utilization [1].

Ammonia offers several advantages over hydrogen, especially in terms of storage and transportation. Unlike H_2, NH_3 benefits from a mature storage and distribution infrastructure [2], is non-flammable, easily liquefiable, and exhibits a high volumetric energy density [3]. Moreover, when integrated with existing infrastructure, NH_3 emerges as a cost-effective alternative, with fuel costs approximately 10.6 – 30.2 times lower than those of H_2 [4]. As a result, several countries have begun to adopt NH_3 as a low-carbon, sustainable fuel within broader energy systems and decarbonization strategies, for example, in internal combustion engines (ICEs) and solid oxide fuel cells (SOFCs) [4]. Notably, in 2020, NH_3 was classified as a "low-carbon fuel" by the U.S. House of Representatives [4].

SOFCs, traditionally operate at temperatures between 600 and 1000 °C [5], are often regarded among the most efficient power generation technologies and have been widely investigated for ammonia-based applications [1]. Although the dissociation of NH_3 reaction is thermodynamically favorable at relatively low temperatures (~185 °C),

* Corresponding author at: TEMA – Centre for Mechanical Technology and Automation, Department of Mechanical Engineering, University of Aveiro, 3810-193 Aveiro, Portugal.
** Corresponding author.
E-mail addresses: duncan@ua.pt (D.P. Fagg), mendes@fe.up.pt (A. Mendes).

https://doi.org/10.1016/j.fuel.2026.139311
Received 21 January 2026; Received in revised form 4 March 2026; Accepted 27 March 2026
Available online 2 April 2026

much higher temperatures are required to achieve practically relevant reacton rates, with kinetic limit for dissociation of ~ 550 °C [6]. Therefore, the high operating temperatures of SOFCs, combined with the use of nickel-yttria stabilized zirconia (Ni-YSZ) cermet as a catalyst [7,8], are particularly attractive for direct ammonia decomposition, enabling the integration of ammonia cracking and electrochemical oxidation within a single device [1]. Nickel serves as both as the anode electronic conductor and as an active catalyst for NH_3 decomposition, while YSZ provides ionic conductivity to the electrode [9,10].

The use of ammonia in fuel cells was first proposed in 1968 by Cairns *et al.* [11] and was subsequently demonstrated by Farr and Vayenas [12,13]. These studies are particularly noteworthy because they show the partial electrochemical oxidation of ammonia can selectively produce nitric oxide (NO) while generating electricity.

More recent studies on direct ammonia solid oxide fuel cells (DA-SOFCs) – *i.e.*, SOFCs operating directly with NH_3 as a fuel – have reported net system-level energy efficiencies of up to 52.1 % in a single-stage process, and up to 72 % for an enhanced system designs incorporating hydrogen membrane separation [14]. Comparable current–potential difference (*I-V*) characteristics have been reported for DA-SOFCs employing conventional Ni-YSZ fuel electrodes relative to H_2-fueled SOFCs [7,15]. Cinti *et al.* [16] reported maximum power density of 240 mW cm^{-2} at 800 °C without observing degradation of failures in the stack. More recently, a study reported high-power density of up to 230 mW cm^{-2} at 680 °C and cell voltage of approximately 0.8 V [17], albeit only for short-term operation. The authors observed failures within the first 50 h of operation and attributed them primarily to nitridation of metalic components due to NH_3 exposure, particularly in ferritic interconnects with high level of chromium, rather than the degradation of the cell microstructure [17]. Another study demonstrated that pre-oxidation treatments and yttria coating of the metallic interconnects can mitigate nitridation effects and improve durability [18].

Ammonia is extensively used in the chemical industry, particularly in the nitric acid (HNO_3) production. In this process, large quantities of nitrous oxide (N_2O), are formed as a by-product and, unless properly treated, are released in the tail gas to the atmosphere [19]. N_2O is of major concern as it is the third most potent greenhouse gas, and therefore, effective mitigation strategies must be impelemted [20]. Currently, catalytic decomposition is typically applied to treat industrial flue gas; however, this approach presents several drawbacks and offers no direct economic benefit [19]. Consequently, combining this waste stream (N_2O) as an oxygen bearing gas with the readily available fuel (NH_3) in a single device (SOFC) could represent an attractive strategy to close the loop in nitric acid production within a sustainable energy conversion process. This envisioned device would promote the electrochemical reduction of N_2O:

$$N_2O(g) + 2e^- \rightarrow N_2(g) + O^{2-} \quad (1)$$

alongside electrochemical oxidation of NH_3:

$$2NH_3(g) + 5O^{2-} \rightarrow 2NO(g) + 3H_2O(g) + 10e^- \quad (2)$$

resulting in the production of nitric oxide (NO) – which is the primary reagent of HNO_3 procuction – N_2O mitigation, and the simultaneous generation of electricity and heat. In the final stage of the process, the produced NO can be recycled into the HNO_3 production cycle to intensify the process. This cogeneration process based on ammonia oxidation and N_2O reduction, also aligns with the principles of economic circularity. Circularity in the chemical industry is gaining momentum, with a focus on sustainable practices, resource reuse, and minimizing environmental impact. By closing material and energy loops, circular chemical processes reduce waste and lower environmental impact.

Farr and Vayenas [12,13] were the first to report the critical role of operating conditions in achieving high selectivity for the NO synthesis during electrochemical direct oxidation of NH_3 – Eq. (2). In particular, they suggested supplying diluted NH_3 as fuel to the SOFC anode. First, dilution helps control the reactor temperature, since the dissociation of pure NH_3 is a highly endothermic process [21,22], and may induce significant thermal gradients across the anode electrode [22]. Second, dilution mitigates material degradation, as pure NH_3 can readily promote the production of nitrides under certain conditions [23]. Additionally, lowering NH_3 concentration enables better control of dissociation kinetics by slowing the reaction rate, thereby preventing catalyst overload and non-uniform fuel utilization [24]. Farr and Vayenas further established that, when NH_3 is employed as the fuel and O_2 as the oxidant, two predominant reactions may occur at the anode: i) the desired direct electrochemical oxidation of ammonia – Eq. (2) –; and ii) a competing chemical reaction in which the electrochemically formed NO reacts with residual NH_3:

$$2NH_3(g) + 3NO(g) \rightarrow \frac{5}{2}N_2(g) + 3H_2O(g) \quad (3)$$

These authors suggested that the rate of the electrochemical reaction – Eq. (2) – was controlled by the diffusion flux of oxygen ions (O^{2-}) across the solid electrolyte, and that the side reaction – Eq. (3) – could be restricted by controlling the ratio between the O^{2-} molar flux and the NH_3 molar flux. To quantify this relationship, they introduced a selectivity factor, *M*, defined as:

$$M = \frac{Q_{O2}}{Q_{NH3}} \quad (4)$$

where Q_{O2} is the molar flow rate of oxygen (mol s^{-1}), and Q_{NH3} is the molar flux of NH_3 (mol s^{-1}). The Q_{O2} is calculated by the Faraday equation:

$$Q_{O2} = \frac{I}{nF} \quad (5)$$

where *I* is the produced current, *n* is the number of electrons (in this case 4), and *F* is the Faraday number (96 485C mol^{-1}).

Parameter *M* therefore represents the O^{2-}/NH_3 ratio at the anode interface, and reflects availability oxygen ions per NH_3 molecule. Under polarization conditions, decreasing the NH_3 concentration at the anode (by dilution) increases *M* value, thereby increasing the relative O^{2-} availability. This shift promotes direct electrochemical oxidation paths, allowing NO formation. Farr and Vayenas [12] found that when *M* equals 0.25, the NO formation becomes to be significant, and that 100 % selectivity is reached for $M \geq 1.25$, suppressing competing side reactions. Therefore, the productivity of NO from NH_3 oxidation is related to parameter *M*.

Building on these findings, the present study aims to gain deeper insight into the performance of a DA-SOFC by extending its operation to diluted NH_3 as the anode fuel and N_2O as the cathode oxidant. The primary objective is to determine whether appropriate operating conditions can be established to enable the simultaneous electrochemical reduction of N_2O at the cathode and electrochemical oxidation of NH_3 toward NO synthesis at the anode. The investigated cell configuration consists of an $Sr_2Fe_{1.5}Mo_{0.5}O_{6-\delta}$ (SFMO) cathode, a promising catalyst for the electrochemical reduction of N_2O [25], a Ni-YSZ anode, a YSZ electrolyte, and a gadolinium-doped ceria (GDC) buffer layer. The latter three components are among the the most widely employed materials in SOFC technology, as reported in [26,27]. The study was conducted at an intermediate operating temperature of 750 °C. Cell performance was evaluated through current–potential difference (*I-V*) characteristerization and polarization experiments, with particular emphasis on optimizing NO production. In addition, the possible reaction pathways governing the electrochemical oxidation of NH_3were systematically investigated to elucidate the underlying mechanism aspects.

2. Experimental

2.1. Preparation and characterization of the SFMO cathode

The $Sr_2Fe_{1.5}Mo_{0.5}O_{6-\delta}$ (SFMO) cathode was prepared by the sol–gel method [28] using stoichiometric amounts of strontium nitrate ($Sr(NO_3)_2$), iron nitrate ($Fe(NO_3)_3$), and ammonium molybdate ($(NH_4)_6Mo_7O_{24}$), (Sigma Aldrich, > 99 %), dissolved in distilled water. Ethylene diamine tetraacetic acid (EDTA) was dissolved in an aqueous ammonia solution (25 %) and subsequently added to the aqueous solution of salts as a gelatin agent, resulting in the formation of black precursors (the solution pH was adjusted to a value of 10); the reaction took place at 90 °C. The resultant powder was calcined at 800 °C (heating/cooling rate of 3 °C min^{-1}, dwell time of 2 h). The calcined powder was milled in an agate mortar, then pressed and further calcined at 1200 °C for 10 h.

X-ray diffraction (XRD) was performed to structurally characterize the produced powder using a *Rigaku SmartLab* diffractometer (Cu Kα radiation – 1.5406 Å, 40 kV, 30 mA). The patterns were obtained in the range $20° < 2\theta < 80°$, with a scan speed of 3° min^{-1}. The Rietveld Refinement was used to extract the lattice parameters, using a pseudo-Voigt peak profile function for profile fitting and a B-spline function for the background.

2.2. Preparation of the membrane electrode assembly (MEA)

The present study used an anode-supported commercial half membrane electrode assembly (MEA) (acquired from Elcogen) with 35 mm diameter, composed of a Ni/YSZ anode (made of 3 layers: active fuel electrode layer – Ni/8YSZ $(ZrO_2)_{0.92}(Y_2O_3)_{0.08}$; support layer Ni/3YSZ $(ZrO_2)_{0.97}(Y_2O_3)_{0.03}$; contact layer NiO, with a total of approximately 300 μm thickness), on top of a 8YSZ electrolyte layer, and a Gadolinia-doped Ceria buffer layer ($Ce_{0.8}Gd_{0.2}O_{2-\delta}$ – CGO20) – Fig. 1. The cathode layer was applied by screen-printer on the CGO20 buffer layer, using a SFMO ink; the ink was prepared by mixing the catalyst powder with a solution of 95 wt% of terpineol with 5 wt% of ethyl cellulose in a 20:80 vol% (powder: solution) ratio. Stearic acid was added to the mixture as a dispersant (3 wt%) – all the compounds were milled in an agate mortar for 15 min. The resultant cathode slurry was screen-printed onto the CGO20 substrate and thermally treated at 350 °C for 1 h to remove the organic binders, followed by sintering at 1000 °C for 4 h in air (with a heating/cooling rate of 1.5 °C min^{-1}). The resulting working electrode areas were 1.77 cm^2.

2.3. Single-cell assembly and characterization

The MEA (SFMO||CGO||YSZ||Ni-YSZ) was assembled in the in-house designed electrochemical reactor (Fig. 2). This reactor consists of two gas compartments corresponding to the anode and the cathode sides, where fuel and oxidant are supplied, respectively. The compartments are physically separated by the prepared MEA, which contains the electrochemically active electrodes. This reactor was sealed with thermiculite gaskets (from Flexitallic) and closed using a torque wrench applying a torque of 0.2 N m [29]. A gold grid and gold wires (from Fiaxell) were used as current collectors on both the cathode and anode sides. Gold paste (from Mateck) was applied to the surfaces of both the cathode and the anode to enhance electrical contact.

2.4. Electrocatalytic tests

The assembled cell reactor was heated to 750 °C at a rate of 0.8 °C min^{-1}, fed with 40 mL min^{-1} of O_2 to the cathode and 30 mL min^{-1} of N_2 to the anode. After temperature stabilization for at least 1 h, the anode was switched to 10 % H_2, balanced with N_2, and maintained for at least 4 h to completely reduce the anode (from NiO to Ni). Then, the cathode was changed to 40 mL min^{-1} of N_2O and the anode was fed with 30 mL min^{-1} of pure/diluted NH_3 (100 %, 50 %, 20 % and 10 % of NH_3 balanced in N_2). The gases used were from Air Liquide: N_2O with a purity of > 99.5 %, H_2 with a purity of 99.995 %, and NH_3 with a purity of 99.96 %.

The electrochemical experiments were performed using an Autolab PGSTAT302N potentiostat/galvanostat. After stabilization at the operating temperature and gas composition, the open circuit potential difference (OCP) was measured. The current–potential difference (*I-V*) characteristics curves were then obtained under potentiostatic control by applying successive potential steps from -0.2 to -0.8 V at a step increment of 5 mV. At the selected potential, the cell was polarized for 15 min, and the corresponding current density was recorded during this period. During electrochemical polarization experiments, the cathode product stream was analysed using a gas chromatograph (GC, Agilent 7890B) to evaluate the N_2O conversion. The anode exiting stream was analysed using a mass spectrometer (MS, Pfeiffer Quasdstar) to determine the concentrations of NO, H_2, NH_3, N_2, and O_2. During the analyses in the MS, a fixed argon flow of 50 mL min^{-1} was used as a reference gas.

After the electrochemical experiments, the *postmortem* microstructure of a fractured cross-section of a MEA was analyzed by Scanning Electron Microscopy (SEM), FEI QUANTA 400 FEG ESEM/EDAX PEGASUS – first MEA – and FEI QUANTA 400 FEG ESEM/EDAX PEGASUS X4M – second MEA. The microscopes were operated at an applied voltage of 15 kV using a backscattered electron (BSE) detector and secondary electrons. Energy-dispersive X-ray spectroscopy (EDS) was performed to determine the elemental composition of the samples.

3. Results and discussion

Fig. 3 depicts the XRD pattern of the $Sr_2Fe_{1.5}Mo_{0.5}O_{6-\delta}$ (SFMO) obtained after calcination at 1200 °C, revealing that no phase impurities are present within the resolution of the employed equipment, suggesting

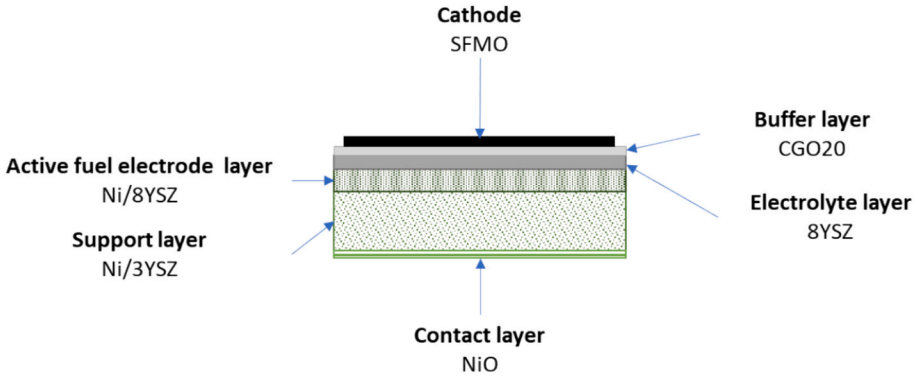

Fig. 1. Scheme representative of the membrane electrode assembly (MEA – SFMO||CGO||YSZ||Ni-YSZ).

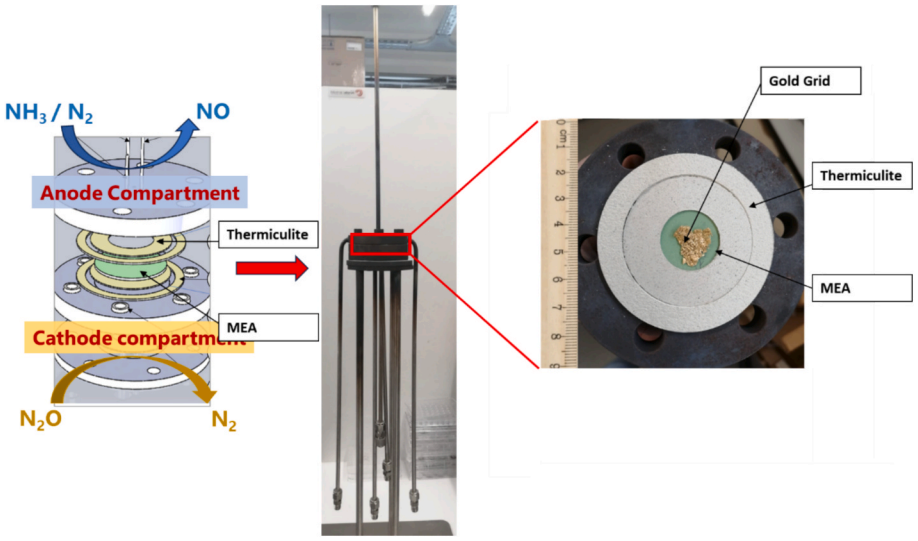

Fig. 2. Image of the reactor used in the electrochemical experiments for NO production.

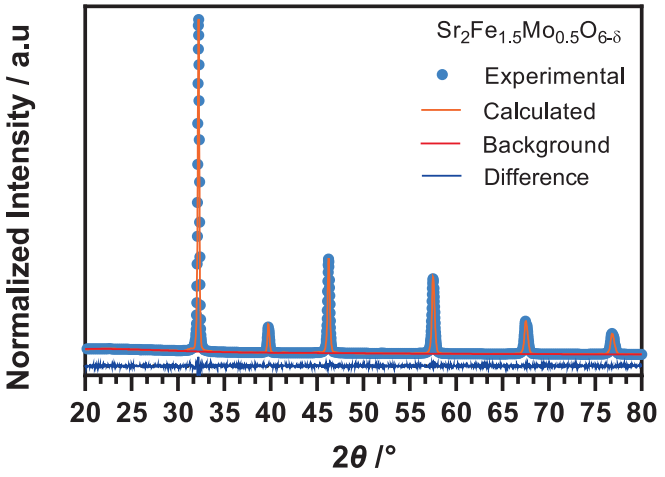

Fig. 3. XRD pattern with Rietveld refinement analysis of SFMO cathode obtained under air atmosphere after calcination at 1200 °C.

that the catalyst was obtained as a pure phase. The prepared cathode exhibits cubic symmetry ($Fm\bar{3}m$ space group), as determined by Rietveld refinement of the XRD data, and confirmed by comparison with the PDF Card No. 01–079-7614. Table 1 depicts the obtained lattice parameters ($a = b = c = 7.8368(8)$ Å), which are in line with those previously reported for this composition [25]. The low χ^2 value in each produced catalyst indicates the good quality of the fit ($\chi^2 = R_{wp}/R_{exp}$).

Table 1
Rietveld refinement extracted parameters of SFMO. R_{wp}, R_{exp}, χ^2, and S are statistical metrics of Rietveld refinement quality.

Material	SFMO
Space Group	$Fm\bar{3}m$(Cubic symmetry)
Lattice parameter ($a = b = c$)/Å	7.8395(1)
Phase angle ($a = b = y$)/°	90
R_{wp}/%	3.86
R_{exp}/%	3.04
χ^2	1.2759
S	1.5659

3.1. Electrochemical NO production from ammonia oxidation coupled with N_2O reduction

Experiments on the electrochemical production of NO from the controlled electrooxidation of ammonia, while promoting electrochemical reduction of N_2O, were conducted using the prepared MEA. Analysis was performed at 750 °C, with 40 mL min^{-1} of N_2O fed to the cathode and 30 mL min^{-1} fed to the anode with mixture of different compositions of NH_3 and N_2.

The OCP was measured previous of each experiment. The obtained values are presented in Table 2.

The OCP values obtained exceeded 1.0 V, for all conditions, indicating good sealing of the ceramic membrane. The slight decrease in the OCP observed under more diluted fuel conditions should be attributed to a reduction in the NH_3 partial pressure.

Following, the current–potential difference (*I-V*) characteristics of the cell under different fuel concentrations were obtained and are plotted in Fig. 4. It should be noted that, for each experiment, the first point of the current–potential difference (*I-V*) characteristics of the cell corresponds to the first polarization potential and not to the OCP.

In Fig. 4, it is observed that the maximum power output obtained with pure fuel was approximately 75 mW cm^{-2}, and the dilution of the fuel reduces the maximum power output, corroborating the findings by Farr and Vayenas [12]. For example, diluting the fuel stream from pure NH_3 to 10 % NH_3/N_2 lowers the maximum power output to 62 mW cm^{-2}. However, this decrease is not as severe as reported by Farr and Vayenas [12]. The cell performance under different fuel dilution conditions is shown in Table 3.

Although state-of-the-art SOFCs operating with hydrogen reaches power densities of *ca.* 1 W cm^{-2} [30], the performance of the present reactor is lower. Previous studies on DA-SOFC have reported peak power densities of approximately 60–100 mW cm^{-2} at 750–800 °C, using Ni-YSZ as anode material, which are of same order of magnitude as the results obtained in the present work [3,21]. Higher performances, ~700

Table 2
Measured OCP values at 750 °C and at different NH_3 concentrations in the fuel stream.

NH_3 concentration/%	OCP/V
100	1.09
50	1.08
20	1.05
10	1.03

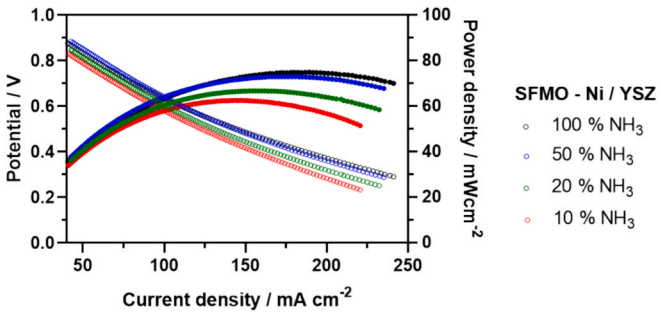

Fig. 4. Current-potential difference (*I-V*) characteristics of the SFMO – Ni/YSZ cell operating at 750 °C, feeding N_2O at the cathode, and fueling the anode with pure and diluted NH_3: 50,20, and 10 % in N_2.

Table 3
Maximum power output of the SFMO – Ni/YSZ cell under different fuel dilution and under different fuel flow rates, operating at 750 °C.

NH_3 concentration/%	Max. Power density/mW cm^{-2}
100	75.011
50	73.065
20	67.793
10	62.586

mW cm^{-2} at 850 °C, have also been reported for better-optimized systems [31]. The comparatively lower power density observed can be attributed to several factors, including the relatively large cathode thickness resulting from manual deposition, as well as the use of NH_3 as fuel and its concentration. At the current stage, however, the primary objective of this work is to prove the concept; systematic device optimization will be addressed in subsequent studies.

After obtaining the current–potential difference (*I-V*) characteristics of the cell, parameter *M* was calculated for each operating condition and depicted in Fig. 5. Each *M* value was determined from current densities measured at different working potentials (0.7, 0.5, 0.4 and 0.35 V) using Eqs. (4) and (5).

As observed in Fig. 5, none of the studied operating conditions resulted in an *M* value ≥1.25; moreover, values of *M* above 0.25 were only computed for the most diluted fuel concentrations of NH_3 – 20 % and 10 % in N_2. As the objective of achieving high selectivity toward NO was not attained, it was decided to further investigate fuel feed dilution to increase the O^{2-}-to-NH_3 ratio. It was then considered 6 vol% NH_3 feed streams to the anode, which has an *M* value of 0.97 at 0.4 V, and a current density of 0.27 A. It is worth noting that high *M* values were only achieved at higher polarization levels, particularly at an applied cell potential of 0.4 V. This condition therefore potentially represents the most favourable regime for promoting selective NO formation.

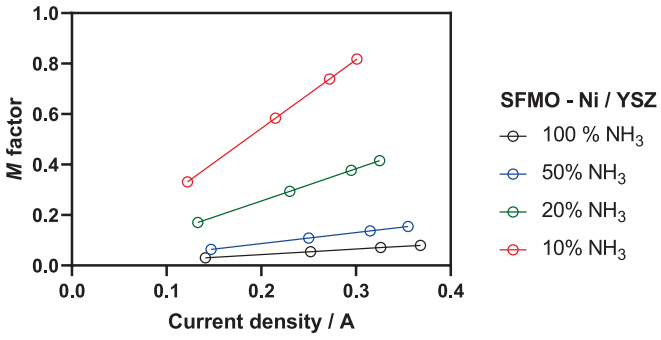

Fig. 5. *M* parameter of the SFMO – Ni/YSZ cell operating at 750 °C feeding N_2O at the cathode, and fueling the anode with pure and diluted NH_3 – 50, 20 and 10 % in N_2.

Accordingly, under all fuel dilution conditions, the fuel cell was polarized at 0.4 V and monitored by chronoamperometry for a total time of 15 min. The results of the polarization experiments are presented in Fig. 6.

The polarization curves obtained during the experiments of electrochemical oxidation of NH_3 in the anode, and electroreduction of N_2O in the cathode, were generally stable. A slight anomaly in the current density is observed at instant approximately 10 min, which remains almost consistent under all operating conditions. The origin of this perturbation could not be conclusively identified; however, the "drop-and-recover" shape suggests a mechanical or physical process rather than a chemical one. Since the events did not change with fuel dilution, they might be likely attributed to systemic characteristics of the reactor geometry or electrode morphology rather than changes in the electrochemical reaction – *e.g.*, accumulation transport of produced water within anode micropores or micro-scale mechanical relaxation of the gold used as current collector (owing to the ductility of the material at operating conditions).

The electrochemical oxidation of ammonia can progress via different pathways, particularly the indirect and direct mechanisms, as schematized in Fig. 7.

The indirect mechanism involves the thermal decomposition of NH_3 to produce 1.5 and 0.5 M ratio of H_2 and of N_2, respectively. Following this route, the generated H_2 would suffer oxidation to water at the anode side (hydrogen oxidation reaction – HOR). The direct mechanism involves the NH_3 direct electrochemical oxidation to N_2 and to H_2O. These two mechanisms should happen simultaneously, with different contributions depending on the operating conditions. Only specific electrochemical conditions, namely high oxygen activity at the anode interface (high *M* value), favour the selective production of NO – direct mechanism. Identifying the relevant operating conditions that favour this mechanism is essential for optimizing the reactor's selectivity towards NO.

To assess this hypothesis, the products of the anodic reaction obtained throughout the polarization tests were continuously monitored by a mass spectrometer. The results from MS analysis are depicted in Table 4.where $Q_{N_{2out}}$ and $Q_{H_{2out}}$ are the reaction product flowrates of N_2 and H_2.

Generally, the reaction product stream composition, obtained by MS, show almost complete NH_3 conversion for all operating conditions (between ~99.09–99.45 %), as illustrated in Table 4. Along with the experiments involving ammonia decomposition, a consistent observation was that the measured H_2 concentrations were often lower than expected, assuming the indirect mechanism, especially at lower levels of fuel dilution, while the measured N_2 values were slightly higher. This difference may indicate that part of the H_2 generated via thermal decomposition was subsequently consumed in surface reactions/electrochemical oxidation – indirect mechanism. This is particularly evident under polarization, where hydrogen oxidation reaction occurs at the cathode, according to the following reaction:

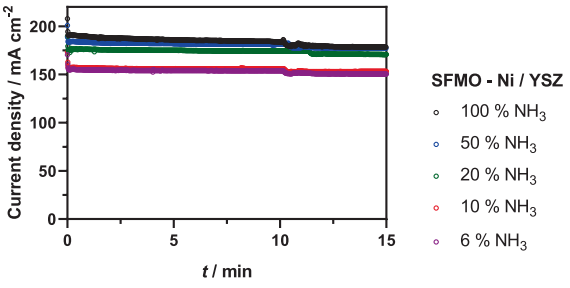

Fig. 6. Chronoamperometry polarization curves of the SFMO – Ni/YSZ cell obtained at 0.4 V, operating at 750 °C, feeding N_2O at the cathode, and fueling the anode with pure and diluted NH_3 (50 vol%, 20 vol%, 10 vol% and 6 vol% in N_2).

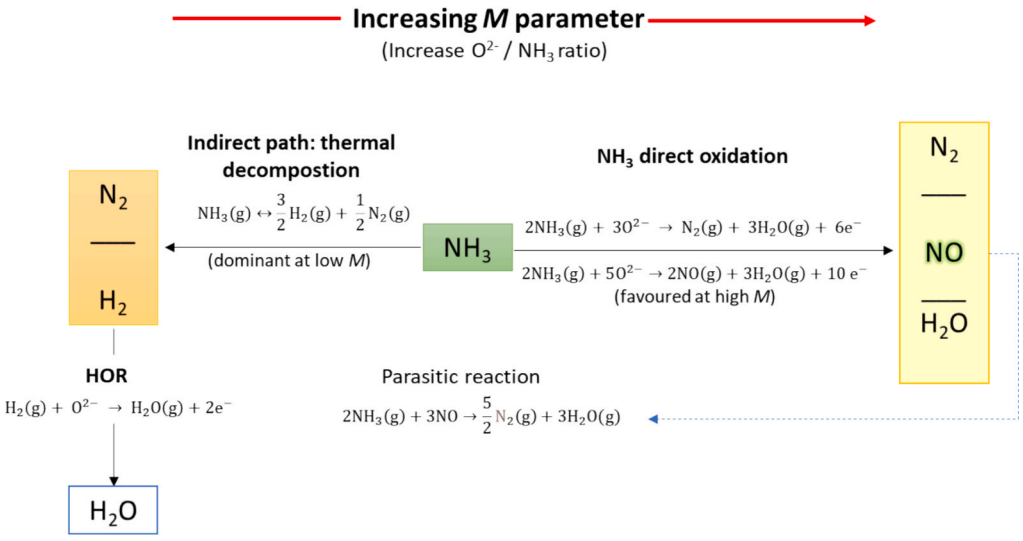

Fig. 7. Scheme on possible pathways for NH_3 oxidation at the anode compartment of the electrochemical cell.

Table 4
Products flow rates expressed as normalized fractions to the initial value measured by the mass spectrometer in the SFMO/Ni-YSZ cell, resulting from the electrocatalytic oxidation of NH_3 combined with the N_2O electrocatalytic reduction of N_2O at a working potential of 0.4 V, operating at 750 °C. The anodic feed was studied from pure NH_3 to various dilution conditions by adjusting the NH_3 concentration in N_2. $Q_{y\ in}$ is the feed molar flowrate, where y is, NH_3, N_2 or H_2; $Q_{y_{out}}$ is the exiting molar flowrate and X_{NH_3} is the reaction conversion of NH_3.

vol% NH_3	$Q_{NH_{3in}}$ /mol min^{-1}	X_{NH_3}/%	Stochiometric flow rates (indirect path)/mol min^{-1}				Measured/%		
			$Q_{N_{2out}}$		$Q_{H_{2out}}$		N_2	H_2	NO
			mol min^{-1}	%	mol min^{-1}	%			
100	1.25×10^{-3}	99.34	6.21×10^{-4}	24.92	1.86×10^{-3}	74.50	25.80	72.79	–
50	6.25×10^{-4}	99.27	3.10×10^{-4}	50.00	9.31×10^{-4}	49.80	53.63	45.64	–
20	2.13×10^{-4}	99.09	1.05×10^{-4}	78.24	3.16×10^{-4}	21.62	81.41	16.80	–
10	1.00×10^{-4}	99.44	4.97×10^{-5}	88.90	1.49×10^{-4}	11.05	88.50	9.99	0.004
6	7.50×10^{-5}	99.45	3.73×10^{-5}	91.36	1.12×10^{-4}	8.61	93.36	5.22	0.006

$$H_2(g) + O^{2-} \rightarrow H_2O(g) + 2e^- \quad (6)$$

This explains why, even though the NH_3 conversion was nearly complete (*e.g.*, ~99.3 %), the H_2 detected downstream was lower than stoichiometrically expected based on the indirect mechanism: part of the thermally produced H_2 is immediately utilized at the anode to produce power, thereby reducing its concentration in the MS effluent stream.

In parallel, the N_2 signal slightly exceeds what was expected based on the direct mechanism, under polarized conditions. This observation may be attributed to the direct electrochemical oxidation of ammonia – or recombination of the adsorbed nitrogenous intermediates – possibly according to the reaction:

$$2NH_3(g) + 3O^{2-} \rightarrow N_2(g) + 3H_2O(g) + 6e^- \quad (7)$$

This pathway contributes to the current generation while bypassing the formation of molecular hydrogen. Consequently, this could explain the lower-than-expected H_2 signals alongside the higher N_2 content observed in the MS analysis.

A notable observation was the detection of NO, under polarized conditions, for the highest fuel dilutions (6 vol% and 10 vol% of NH_3), corresponding to higher M values. This suggests that an additional electrochemical oxidation pathway of NH_3 is taking place, likely involving the direct formation of NO via a 5-electron process – Eq. (2).

Such a reaction would bypass the formation of H_2 and N_2 intermediates, directly consuming NH_3 and contributing to the generation of electrical current. This mechanism could also explain the lower-than-predicted H_2 and N_2 levels at 10 vol% of NH_3, suggesting that higher NH_3 concentration suppresses direct electrochemical oxidation due to lower relative availability of O^{2-} at the anode interface. Interestingly, at 6 vol% of NH_3 feed yield a higher quantity of NO, but also delivered a greater value of measured N_2 compared to the expected. This suggests that a parasitic chemical reaction between NO and unreacted NH_3 might be occurring – Eq. (3).

This may be attributed to the increased O^{2-}/NH_3 ratio (high M value) which accelerates NO formation and creates a local environment rich in both product (NO) and some unreacted fuel (NH_3). However, some NO is partially offset by secondary catalytic reduction. This shift, combined with the stabilization of the local thermal profile by the increased N_2 ballast, provides the necessary kinetic window for the parasitic reduction of NO to N_2, as confirmed by the concurrent increase in N_2 levels beyond the feed concentration.

The produced NO could also have been produced by direct N_2 electrochemical oxidation:

$$N_2(g) + O^{2-} \rightarrow 2NO(g) + 2e^- \quad (8)$$

or its direct chemical oxidation:

$$N_2(g) + O_2 \rightarrow 2NO(g) \quad (9)$$

However, the direct oxidation of NH_3 is energetically more favorable than the oxidation of N_2, since the bound dissociation of molecular N_2 requires much more energy than NH_3 (*ca.* 942 kJ mol^{-1} *vs* 347 kJ mol^{-1}) [32]. Moreover, the chemical oxidation of N_2 is not favorable under cell operating conditions as this process typically occurs at temperatures above 1200 °C [33].

To further understand the contribution of the fuel to the current generation, the fuel utilization (U_f) was calculated as a means of correlating the fed NH_3 consumed for power production via

electrochemical oxidation [34]. Fuel utilization was calculated as following:

$$U_f = \frac{I}{Fnm_{fuel}} \quad (10)$$

where I is the current (A), n is the number of electrons released per mole of fuel, and m_{fuel} is the NH_3 fed (mol s^{-1}).

Due to the coexistence of multiple reaction pathways occurring simultaneously in the anode compartment, the interpretation of the fuel utilization (U_f) obtained value requires careful consideration, since both indirect and direct mechanisms take place. This may directly contribute to the power generation distinctly. These competing reactions lead to different electron transfer numbers per mole of fuel involved: while H_2 oxidation involves 2 electrons per mole (indirect mechanism), the direct oxidation of NH_3 can involve up to 3 or 5 electrons per mole of NH_3 converted – *cf.* Eqs. (2) and (7). However, the dominant electrochemical oxidation mechanism of NH_3 is the direct pathway, described by the overall reaction Eq. (7), which effectively combines both NH_3 thermal decomposition and HOR – Eq. (6). Consequently, an effective value of $n = 3$ electrons per mole of NH_3 was used consistently, reflecting the net electron transfer per mole of NH_3 consumed for this stated reaction. The calculated U_f values for this case study are presented in Table 5.

Generally, the U_f increases as the fuel dilution in the anode increases, reaching a maximum of 75.56 % when 6 % of NH_3 was fed to the anode.

Although the NH_3 conversion shown in Table 4 levels out for the two highest NH_3 dilutions (10 and 6 %), the U_f value in Table 5 increases across the entire dilution range. This apparent inconsistency may be justified as the NH_3 conversion reflects the extent of chemical decomposition, whereas fuel utilization quantifies the fraction of the supplied fuel that is electrochemically oxidized. In this sense, as NH_3 is diluted by mixing with nitrogen, a decrease in its effective thermal decomposition can be expected [35], according to Le Chatelier's principle, which would shift the ammonia decomposition reaction to the left side. This would explain the observed initial decrease in NH_3 conversion, as observed in Table 4, until 20 vol% feed dilution. Conversely, at lower NH_3 concentrations, a higher fraction of NH_3 is electrochemically oxidized, as evidenced by the increasing deviation between measured and expected H_2 – indirect mechanism; higher N_2 and NO concentrations, Table 4.

The nitrous oxide conversion was also evaluated along with the polarization experiments. A gas sample from the cathode was collected and injected into the GC at instant 10 min of the reaction. The N_2O conversion was calculated based on:

$$X_{N_2O} = \frac{Q_{N_2O_{in}} - Q_{N_2O_{out}}}{Q_{N_2O_{in}}} \quad (11)$$

where X_{N_2O} is the conversion of N_2O, and $Q_{N_2O_{in}}$ and $Q_{N_2O_{out}}$ are the molar fraction of nitrous oxide entering and leaving the cathode, respectively. The conversion of N_2O obtained for different fuel concentrations is presented in Table 6.

The N_2O conversion at the cathode under cell polarization yields a modest result, with values ranging from 8 % to 10 %, as the fuel concentration at the anode is varied from 6 % to 100 %. However, the obtained conversions are always higher than those at OCP conditions (conversion of ~5.9 %), suggesting that electrochemical promotion of N_2O reduction does occur.

Table 5
Fuel utilization calculation based on the assumption that the number of electrons participating in electrochemical reactions is 3, for the experiments performed at 0.4 V and 750 °C.

NH_3 concentration/vol%	U_f/ %
100	5.45
50	10.72
20	30.36
10	57.40
6	75.56

Table 6
Conversion of nitrous oxide obtained in the cathode at different fuel concentrations in the anode, operating at 750 °C.

Cell condition	NH_3 concentration/%	X_{N_2O}/%
OCP	100	5.90
0.4 V	100	9.67
	50	9.51
	20	8.31
	8	8.09
	6	8.09

The conversion of N_2O decreases as the fuel concentration at the anode decreases. In fact, the cathodic reaction kinetics Eq. (1) is related to the electronic current measured at the external circuit. Then, the oxidation reaction plays a crucial role in the electrochemical reduction of N_2O at the cathode by providing the necessary current load. The observed decrease in N_2O conversion with increasing fuel dilution at the anode can be rationalized by a slight reduction in the electrochemical activity of the cell.

N_2O is a chemically stable molecule that undergoes reduction only slowly unless electrochemically driven [36]. Additionally, atomic oxygen derived from N_2O that adsorbs on the catalyst surface hinders the catalytic activity of the SFMO perovskite. This inhibition is associated with the low desorption rate of atomic oxygen via recombination to form molecular oxygen, thereby making high N_2O conversion difficult to achieve [36]. In this sense, the continuous consumption of surface oxygen species could effectively overcome this limitation and facilitate the regeneration of active surface sites, thereby promoting N_2O conversion. To overcome this limitations, some Co/Fe-based perovskite oxides have been developed, as $Ba_{0.5}Sr_{0.5}Co_{0.8}Fe0.2O_{3-\delta}$ and $PrBaCo_2O_{5+\delta}$ [36]; however, their high coefficients of thermal expansion have hindered practical application.

These observations indicate significant room for performance improvement, either through optimization of the cathode material, enhancement of operating conditions (*e.g.*, potential difference and temperature), or refinement of cathode deposition techniques.

3.2. Post-mortem analysis

The microstructure of the SFMO||CGO||YSZ||Ni-YSZ cell, after the polarization experiments for NO production, was analyzed by scanning electron microscopy (SEM) to assess morphological aging of the electrodes. Fig. 8a shows the electrode before testing, while Fig. 8b and Fig. 8c presents the *post-mortem* top view of the anode side of MEA, where electrochemical oxidation of NH_3 takes place. The top-view morphology of the anode surface reveals a rice-starch-like morphology, with some agglomeration, typical of a Ni anode cermet [37].

SEM images of the anode functional layer generally reveal the presence of black voids in the used MEA (Fig. 8b and Fig. 8c), compared to the pristine NiO-YSZ (Fig. 8a), which is characteristic of the *in-situ* reduction of the NiO to metallic Ni – a process essential for creating the electronic conductivity and active sites required for NH_3 oxidation [38]. While prolonged exposure to high temperatures resulted in some degree of Ni sintering, the microstructure remained largely intact. Notably, there was no evidence of significant micropore formation or severe agglomeration, which is commonly observed in structures degraded by nickel nitride (Ni_3N) formation [23]. This suggests that the anode maintains structural stability under the tested electrochemical conditions.

Fig. 9 presents the fractured cross-section view of the MEA *post-mortem*. Fig. 9a illustrates the different layers of the MEA: Z1) anode

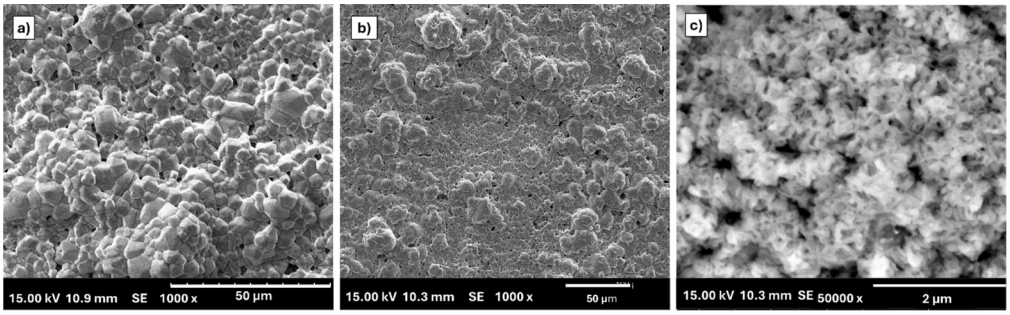

Fig. 8. SEM images of the Ni-YSZ anode in a top view: a) NiO-YSZ before the experiment, b) and c) Ni-YSZ *post-mortem* (for consistent visual comparison, scale bar of image b) was normalized to 50 µm).

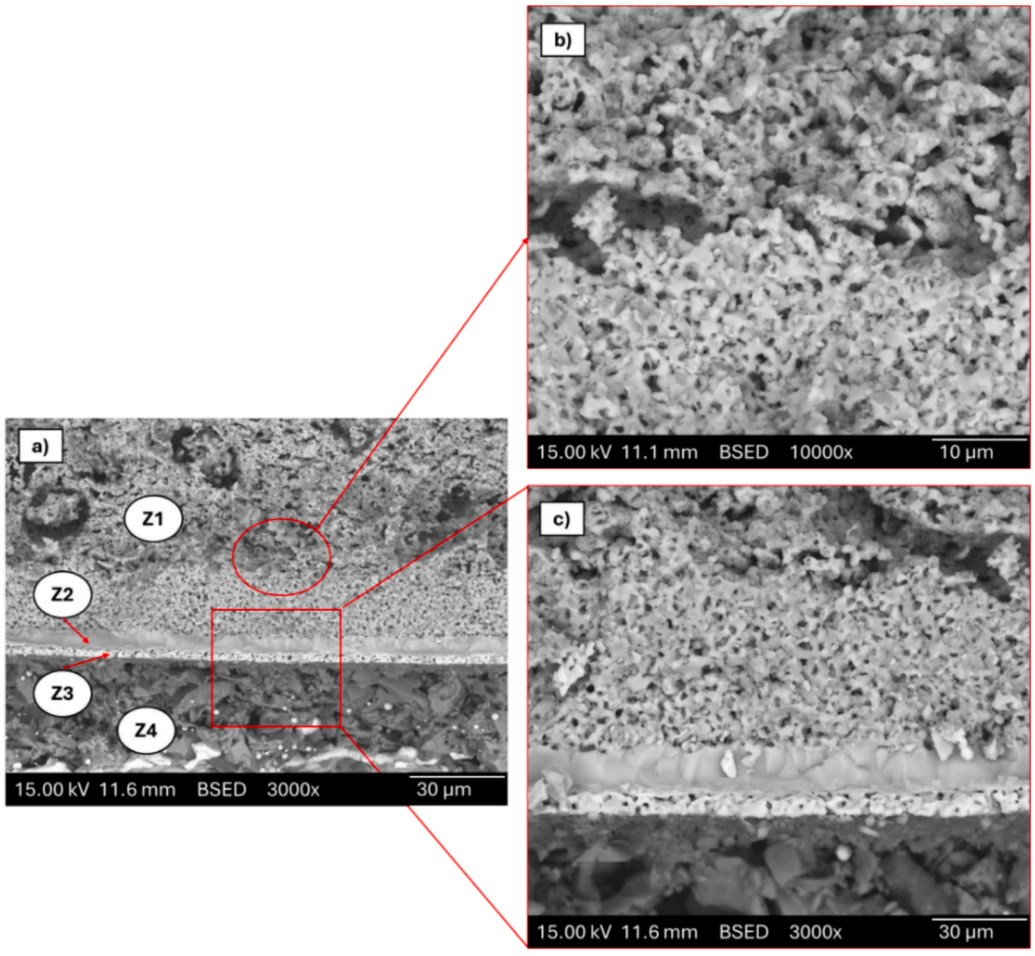

Fig. 9. Scanning electron microscopy images (SEM) of cross-section microstructure of the MEA after reduction: Z1: anode – Ni-YSZ, Z2: electrolyte – YSZ, Z3: buffer layer and Z4: cathode – SFMO.

made of a cermet of Ni-YSZ, Z2) electrolyte layer composed of YSZ, Z3) buffer layer of CGO, and Z4) cathode layer made of the produced SFMO.

The cross-section SEM image of the Ni-YSZ anode layer reveals a distinct bilayer structure, with a denser region adjacent to the electrolyte (Fig. 9c) and a more porous layer at the outer surface (Fig. 9b). Both layers displayed similar oxidation states – composition on oxygen, as determined by EDS, which arose due to the naturally existing oxygen atoms in the YSZ structure and due to the cool down of the cell under non-reducing atmosphere – and show similar Ni concentration. This bilayer is consistent with the architecture of the commercial Elcogen MEA, which comprises the active anode electrode layer (Ni-8YSZ, inner layer) and the support layer (Ni-3YSZ, outer layer) – (cf. Fig. 1). The image in Fig. 9c shows no delamination between electrodes and electrolyte/buffer layers. Moreover, there is no observation of strontium zirconate ($SrZrO_3$) in zones 3, 4, and 5 in Fig. 10d–e, indicative that strontium did not diffuse from the cathode through the GDC buffer layer (zone 4 in Fig. 10a) to react with the YSZ electrolyte – EDS results in Fig. 10d and Fig. 10e.

4. Conclusions

This work advances the investigation of direct-ammonia solid oxide fuel cells as a strategy to reduce N_2O emissions, while simultaneously valorizing this waste by producing nitric oxide (NO) – the primary

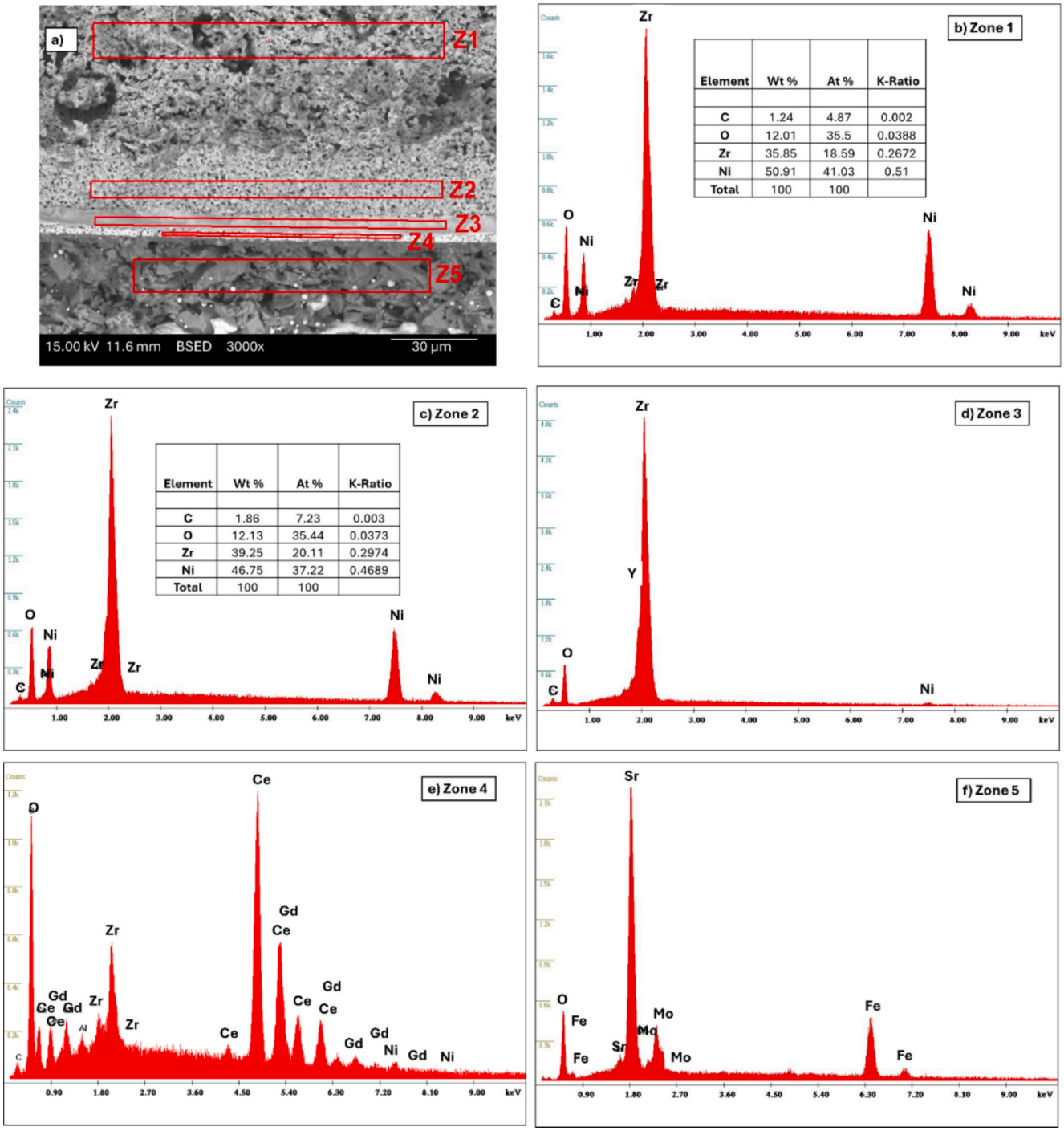

Fig. 10. EDS analysis images of cross-section microstructure of the MEA: Z1: anode – Ni-YSZ, Z2: electrolyte – YSZ, Z3: buffer layer and Z4: cathode – SFMO.

precursor for HNO_3 synthesis. Specifically, the study focused on the behavior of the anode under different fuel compositions, varying the anode feed from pure NH_3 to 6 % NH_3 balanced with N_2. The results revealed a complex interplay between fuel dilution, reaction pathways, and electrochemical performance.

An increase in fuel dilution had only a minor impact on the performance of the SOFC: reducing the ammonia concentration from 100 % to 10 % (maintaining volumetric flow rate at 30 mL min^{-1}), at 750 °C and 0.4 V, decreased the power density from 75 to 62 mW cm^{-2}, while fuel utilization increased. The results provide insight into the mechanisms of NH_3 oxidation, indicating that NH_3 proceeds simultaneously through both indirect (via H_2 and N_2 formation and subsequent electrochemical H_2 oxidation to H_2O) and direct electrochemical mechanisms, involving the formation of N_2, NO, and H_2O. The low-than-expected H_2 formation under polarized conditions may explains the indirect route. The detection of NO, observed exclusively at higher fuel dilutions (6–10 vol% NH_3), confirms the activation of a direct electrochemical oxidation pathway. This observation correlates with an increase in the O^{2-}/NH_3 molar ratio (*M* factor), which promotes more effective interaction between oxide ion flux and available fuel, thereby favoring electrochemical oxidation over parallel pathways, In these conditions, cell exhibited the highest NH_3 conversion (~99.45 %) and fuel utilization (~75.56 %).

Higher dilutions favor deep oxidation to NO, although secondary gas-phase reactions may compete at specific concentrations (*e.g.*, 6 vol %), highlighting the complexity of NH_3 oxidation and the interplay of

factors dictate the final effluent composition. Although the absolute amount of NO produced remained low, these findings validate the proposed concept and establish a promising basis for further investigation into selective NO formation pathways.

The electrochemical decomposition of pure N_2O (40 mL min^{-1}) reached approximately 10 % at 0.4 V and 750 °C. While modest, this result is significant considering the high thermal stability of N_2O and highlights the benefits of electrochemical promotion. Further optimization and mechanistic studies are required to improve cathodic performance.

Overall, the results demonstrate the robustness of the Ni-YSZ anode under a wide range of fuel compositions, supporting its suitability for flexible operation and reinforcing the potential of ammonia-fueled SOFCs for integrated energy generation and chemical valorization.

CRediT authorship contribution statement

Celina Fernandes: Writing – original draft, Methodology, Investigation, Formal analysis, Data curation, Conceptualization. **Laura I.V. Holz:** Writing – review & editing, Funding acquisition. **Francisco J.A. Loureiro:** Writing – review & editing, Funding acquisition. **Sergey M. Mikhalev:** Investigation, Formal analysis. **Fátima Santos:** Writing – review & editing. **Duncan P. Fagg:** Writing – review & editing, Supervision, Resources, Funding acquisition. **Adélio Mendes:** Writing – review & editing, Supervision, Resources, Project administration, Funding acquisition.

Declaration of Competing Interest

The authors declare that they have no known competing financial interests or personal relationships that could have appeared to influence the work reported in this paper.

Acknowledgments

This work was supported by national funds through FCT/MECI: LEPABE, UID/00511/2025 (https://doi.org/10.54499/UID/00511/2025) and UID/PRR/00511/2025 (https://doi.org/10.54499/UID/PRR/00511/2025) and ALiCE, LA/P/0045/2020 (https://doi.org/10.54499/LA/P/0045/2020). This work is a result of project HI_MOV – "Corredor Tecnológico Transfronterizo de Movilidad com Hidrógeno Renovable", with reference 0160_HI_MOV_1_E, cofinanced by European Regional Development Fund (ERDF), through Programa de Cooperação INTERREG VI A Espanha – Portugal (POCTEP) 2021-2027.

Celina Fernandes wants to acknowledge to FCT for the PhD grant 2021.07014.BD; Laura Holz, Francisco Loureiro and Fátima Santos acknowledge to FCT for the CEEC grants 2023.05868.CEECIND (10.54499/2023.05868.CEECIND/CP2840/CT0021), 2020.02797.CEECIND/CP1589/CT0030 (10.54499/2020.02797.CEECIND/CP1589/CT0030) and 2023.07366.CEECIND/CP2834/CT0012 (10.54499/2023.07366.CEECIND/CP2834/CT0012), respectgively.

The authors also acknowledge the projects with references: 2022.09319.PTDC (10.54499/2022.09319.PTDC), 2022.02498.PTDC (10.54499/2022.02498.PTDC) from Fundação para a Ciência e a Tecnologia (FCT) and the projects COMPETE2030-FEDER-00744500 16284 2023.17866.ICDT (https://doi.org/10.54499/2023.17866.ICDT) and COMPETE2030-FEDER-00770000 16527 2023.17134.ICDT. This work is also funded by national funds through FCT – Fundação para a Ciência e a Tecnologia, I.P., under the project/contract UID 00481 – Centre for Mechanical Technology and Automation.

Data availability

Data will be made available on request.

References

[1] Jeerh G, Zhang M, Tao S. Recent progress in ammonia fuel cells and their potential applications. J Mater Chem A Mater 2021;9(2):727–52. https://doi.org/10.1039/D0TA08810B.
[2] Osman AI, et al. Hydrogen production, storage, utilisation and environmental impacts: a review. Environ Chem Lett Feb. 2022;20(1):153–88. https://doi.org/10.1007/s10311-021-01322-8.
[3] Fournier GGM, Cumming IW, Hellgardt K. High performance direct ammonia solid oxide fuel cell. J Power Sources Nov. 2006;162(1):198–206. https://doi.org/10.1016/j.jpowsour.2006.06.047.
[4] Cheng Q, Muhammad A, Kaario O, Ahmad Z, Martti L. Ammonia as a sustainable fuel: Review and novel strategies. Renew Sustain Energy Rev Jan. 2025;207:114995. https://doi.org/10.1016/j.rser.2024.114995.
[5] Dharini T, Kuppusami P, Kirubaharan AMK. Nanocomposite ceramic diffusion barrier coatings for nuclear vitrification furnace. Adv Ceram Coat Elsevier 2023:357–80. https://doi.org/10.1016/B978-0-323-99659-4.00020-6.
[6] A. Roine, "HSC Chemistry® [Software]," 2021, Metso Outotec. [Online]. Available: https://www.mogroup.com/hsc.
[7] Ma Q, Ma J, Zhou S, Yan R, Gao J, Meng G. A high-performance ammonia-fueled SOFC based on a YSZ thin-film electrolyte. J Power Sources Jan. 2007;164(1):86–9. https://doi.org/10.1016/j.jpowsour.2006.09.093.
[8] Zhong F, et al. Site-oriented design of spinel MgxNiMn2-xO4-δ as cathode material of intermediate-temperature direct ammonia solid oxide fuel cell. J Power Sources Aug. 2021;503:230020. https://doi.org/10.1016/j.jpowsour.2021.230020.
[9] Luo Y, et al. Coupling ammonia catalytic decomposition and electrochemical oxidation for solid oxide fuel cells: a model based on elementary reaction kinetics. J Power Sources May 2019;423:125–36. https://doi.org/10.1016/j.jpowsour.2019.03.064.
[10] Li T, Ling Y, Lin B, Ou X, Wang S. A simple, feasible, and non-hazardous laboratory evaluation of direct ammonia solid oxide fuel cells fueled by aqueous ammonia. Sep Purif Technol Sep. 2022;297:121511. https://doi.org/10.1016/j.seppur.2022.121511.
[11] Cairns EJ, Simons EL, Tevebaugh AD. Ammonia–oxygen fuel cell. Nature Feb. 1968;217(5130):780–1. https://doi.org/10.1038/217780a0.
[12] C. G. Vayenas and R. D. Farr, "Cogeneration of electric energy and nitric oxide," Science (1979)., vol. 208, no. 4444, pp. 593–594, May 1980, doi: 10.1126/science.208.4444.593.
[13] Farr RD, Vayenas CG. Ammonia high temperature solid electrolyte fuel cell. J Electrochem Soc Jul. 1980;127(7):1478–83. https://doi.org/10.1149/1.2129934.
[14] Selvam K, Komatsu Y, Sciazko A, Kaneko S, Shikazono N. Thermodynamic analysis of 100% system fuel utilization solid oxide fuel cell (SOFC) system fueled with ammonia. Energy Convers Manag Dec. 2021;249:114839. https://doi.org/10.1016/j.enconman.2021.114839.
[15] Molouk AFS, Okanishi T, Muroyama H, Matsui T, Eguchi K. ElecTROCHEMICAL AND CATALYTIC BEHAVIORS of Ni–YSZ anode for the direct utilization of ammonia fuel in solid oxide fuel cells. J Electrochem Soc 2015;162(10):F1268–74. https://doi.org/10.1149/2.1011510jes.
[16] Cinti G, Discepoli G, Sisani E, Desideri U. SOFC operating with ammonia: Stack test and system analysis. Int J Hydrogen Energy 2016;41(31):13583–90. https://doi.org/10.1016/j.ijhydene.2016.06.070.
[17] Machaj K, et al. Studies of ammonia-fueled SOFC stacks: Insights into possible failure causes. Fuel Feb. 2026;405:136579. https://doi.org/10.1016/j.fuel.2025.136579.
[18] Talic B, Larring Y, Stange M, Rørvik PM. Nitridation of solid oxide fuel cell interconnects in ammonia: effect of protective coatings and pre-oxidation. J Electrochem Soc Feb. 2026;173(3):034503. https://doi.org/10.1149/1945-7111/ae3d8b.
[19] Alves L, et al. A comprehensive review of NOx and N2O mitigation from industrial streams. Renew Sustain Energy Rev Mar. 2022;155:111916. https://doi.org/10.1016/j.rser.2021.111916.
[20] Tian H, et al. Global methane and nitrous oxide emissions from terrestrial ecosystems due to multiple environmental changes. Ecosyst Health Sustainability Mar. 2015;1(1):1–20. https://doi.org/10.1890/EHS14-0015.1.
[21] Elmutasim O, Dhawale DS, Giddey S, Paul G, Bhattacharya S. Unravelling the reaction mechanism on Ni–YSZ anode supported direct ammonia solid fuel cell: Experimental and theoretical studies. Appl Surf Sci Mar. 2025;686:162175. https://doi.org/10.1016/j.apsusc.2024.162175.
[22] Wang D, Wang L, Liu Y, Zhang X, Liu Z. Study of thermal effects in ammonia-fueled solid oxide fuel cells. J Electroanal Chem Jan. 2024;953:118001. https://doi.org/10.1016/j.jelechem.2023.118001.
[23] Dhawale DS, Biswas S, Kaur G, Giddey S. Challenges and advancement in direct ammonia solid oxide fuel cells: a review. Inorg Chem Front 2023;10(21):6176–92. https://doi.org/10.1039/D3QI01557B.
[24] Cinti G, Baldinelli A, Bidini G, Barelli L. Electrochemical impedance spectroscopy study on ammonia-fed solid oxide fuel cells. J Phys Conf Ser Dec. 2022;2385(1):012052. https://doi.org/10.1088/1742-6596/2385/1/012052.
[25] Holz LIV, et al. Strontium iron molybdenum oxide as electrocatalyst for nitrous oxide reduction in solid oxide fuel cells. Int J Hydrogen Energy Feb. 2024;54:25–36. https://doi.org/10.1016/j.ijhydene.2023.05.251.
[26] Shaikh SPS, Muchtar A, Somalu MR. A review on the selection of anode materials for solid-oxide fuel cells. Renew Sustain Energy Rev Nov. 2015;51:1–8. https://doi.org/10.1016/j.rser.2015.05.069.

[27] Vinchhi P, Khandla M, Chaudhary K, Pati R. Recent advances on electrolyte materials for SOFC: a review. Inorg Chem Commun Jun. 2023;152:110724. https://doi.org/10.1016/j.inoche.2023.110724.
[28] Santos JRD, et al. Understanding the cathodic polarisation behaviour of the misfit [Ca2CoO3−δ]q[CoO2] (C349) as oxygen electrode for IT-SOFC. Electrochim Acta Sep. 2018;285:214–20. https://doi.org/10.1016/j.electacta.2018.08.018.
[29] Fernandes C, Alves L, Holz L, Fagg D, Mendes A. A simple compression sealing method for planar single-cell SOFC testing. Fuel Dec. 2025;402:135872. https://doi.org/10.1016/j.fuel.2025.135872.
[30] E. D. Wachsman and K. T. Lee, "Lowering the temperature of solid oxide fuel cells," Science (1979)., vol. 334, no. 6058, pp. 935–939, Nov. 2011, doi: 10.1126/science.1204090.
[31] Hagen A, Langnickel H, Sun X. Operation of solid oxide fuel cells with alternative hydrogen carriers. Int J Hydrogen Energy Jul. 2019;44(33):18382–92. https://doi.org/10.1016/j.ijhydene.2019.05.065.
[32] B. de B. Darwent, Bond dissociation energies in simple molecules. National Standard reference data system , 1970.
[33] Babcock & Wilcox Enterprise, "The B&W Learning Center For a net-zero future - Leading the world in clean power production technology." Accessed: Jul. 30, 2025. [Online]. Available: https://www.babcock.com/home/about/resources/learning-center/nitrogen-oxides-nox-primer#:~:text=Significant%20levels%20of%20NOx%20are%20usually%20formed%20above,states%20and%20participate%20in%20a%20series%20of%20reactions.
[34] Barelli L, Bidini G, Cinti G. Operation of a solid oxide fuel cell based power system with ammonia as a fuel: experimental test and system design. Energies (Basel) Nov. 2020;13(23):6173. https://doi.org/10.3390/en13236173.
[35] Holz LIV, et al. Vanadium (oxy)nitride as a new category of anode for direct ammonia solid oxide fuel cells cells. Renew Energy Dec. 2022;201:124–30. https://doi.org/10.1016/j.renene.2022.10.098.
[36] Rong Y-T, et al. Efficient power generation in a solid oxide fuel cell using N2O as the oxidant. Rare Met Aug. 2025;44(8):5859–67. https://doi.org/10.1007/s12598-025-03305-y.
[37] B. Shri Prakash, S. Senthil Kumar, and S. T. Aruna, "Properties and development of Ni/YSZ as an anode material in solid oxide fuel cell: A review," Renewable and Sustainable Energy Reviews, vol. 36, pp. 149–179, Aug. 2014, doi: 10.1016/j.rser.2014.04.043.
[38] Jeangros Q, et al. Reduction of nickel oxide particles by hydrogen studied in an environmental TEM. J Mater Sci Apr. 2013;48(7):2893–907. https://doi.org/10.1007/s10853-012-7001-2.